

1                    Medical Image Compression Based on Singular Value  
2                    Decomposition

3                    Hyobin Cho \*<sup>1</sup> and Soomin Jeon<sup>2</sup>

4                    <sup>1</sup>University of Pittsburgh

5                    <sup>2</sup>Dong-A University

6                    **Abstract**

7                    In a landscape abundant with diverse volumetric digital data, the imperative to cultivate  
8                    an advanced compression methodology geared towards impeccable image storage and seam-  
9                    less reconstruction has grown significantly. The twin focal points of image compression lie in  
10                  preserving image fidelity post-compression while concomitantly minimizing image dimensions.  
11                  This study delves into harnessing one of the pivotal tenets of Linear Algebra, Singular Value  
12                  Decomposition (SVD), to intricately fine-tune the compression quotient for medical imagery  
13                  encompassing X-rays and Magnetic Resonance Images (MRIs).

14                  The core contribution of this research materializes in the formulation of an optimal com-  
15                  pression threshold substantiated by a suite of credible image quality assessment metrics. This  
16                  approach endeavors to strike an equilibrium between efficient data utilization and perceptually  
17                  faithful image restoration.

18                  **keywords:** Medical Image Compression, Singular Value Decomposition, Image quality preser-  
19                  vation, Optimal Rank

20                  **1 Introduction**

21                  Nowadays, images are stored in and transmitted through digital devices such as computers,  
22                  laptops, or smartphones. As digital imaging technology is growing continuously in different applica-  
23                  tions such as personal, entertainment, education, remote sensing, and medical fields, high-resolution  
24                  images with high visual quality are more commonly produced and utilized in the corresponding  
25                  fields. [1] Since these high-resolution images require a large amount of storage space due to their big  
26                  data size, it has become more necessary to resolve the problems in data storage and transmission  
27                  caused by the big data size of the images. And, this problematic situation has elicited different kinds  
28                  of data compression techniques which represent a big image file into a smaller file with fewer data. [2]

---

\*23 Summer Research in the Computational Mathematics and Medical Imaging Laboratory (CMMI Lab) of Dong-A University, Busan, Republic of Korea  
Hyobin Cho: hyc32@pitt.edu, Soomin Jeon: soominjeon@dau.ac.kr

29

30     The image compression schemes are normally divided into two big categories: lossless com-  
31     pression and lossy compression. The lossless compression doesn't change the data of the original  
32     image which means there is no degradation in image quality, but has less compression ratio than  
33     the lossy compression. The lossy compression is used to minimize the needed storage by the images.  
34     As a result, there is a trade-off between the level of compression and the quality of the image after  
35     reconstruction. [3] Also, the lossless technique can completely retrieve the original data from the  
36     compressed image, but retains a compression ratio of around 2 to 4%. [4] In lossy compression, the  
37     compressed image must be visually lossless and the size of the compressed image should be reduced  
38     significantly at the same time. The quality of the compressed image is assessed with appropriate  
39     error assessment metrics such as L1/L2 error, SSIM, and PSNR. Huffman coding, Run-length encod-  
40     ing, arithmetic coding, dictionary techniques, and Bit Plane coding are typical examples of lossless  
41     compression techniques. PNG and GIF are one of the most common lossless image formats. JPEG  
42     which uses Discrete Cosine Transform(DCT) as its compression technique is an example of lossy  
43     compression.[5] Digital Imaging and Communication in Medicine (DICOM) proposes the standard  
44     for the management and communication of medical images. And the examples of the approved  
45     compression algorithms are JPEG, JPEG 2000, and Wavelet Transforms. [6]

46

47     To overcome the disadvantages of lossy and lossless compression techniques, the hybrid com-  
48     pression technique has been invented as well. The hybrid compression techniques divide the total  
49     area into two disjoint areas, the Area of Interest (AOL) and the outside regions of interest. To  
50     achieve this partition, image segmentation needs to be done to extract the region of interest through  
51     either automatic or semi-automatic processes. [7] This implies that the hybrid compression tech-  
52     niques compress the ROI areas with lossless methods and compress the non-ROI areas with lossy  
53     methods. The hybrid compression has its advantages in that it only maintains the important in-  
54     formation that is diagnostically significant and compresses the other parts; however, it yields the  
55     complexity in the algorithms for image segmentation and the necessity to develop new appropriate  
56     hybrid techniques for different uses. More recently, the medical society started using Compressed  
57     Sensing (CS) to compress medical images. CS accelerates data acquisition and enables a credible,  
58     time-resolved measurement of the ultrafiltration progress. [8] On top of that, CS has been adapted  
59     as an alternative reconstruction method by using the sparsity of MRI scans to randomly undersam-  
60     ple the k-space and consequently saving process time. [9] However, using high acceleration sensing  
61     with high resolution can lead to some disadvantageous circumstances where image quality decreases  
62     due to insufficient noise removal. [10] Overall, there has not been proposed a finalized version of  
63     the optimal compression technique for medical images. Thus, we focused on how to overcome the  
64     disadvantages that lossless and hybrid compression techniques have by delving into the fundamental  
65     structure and the results of lossy compression on medical imaging.

66

67     The main reason for the possibility of clinical application of the lossy compression techniques is  
68     that the medical applications tolerate some loss of information from the original data as long as it  
69     doesn't raise any significant errors in analysis and diagnosis. [11]. In addition, previous studies have

70 shown that the diagnostically significant and important information is localized in a relatively small  
 71 area which is about 5 to 10% of the total area of an image.[12] Moreover, since it is essential to  
 72 maintain the rigid similarity of the compressed image with the original image, to reduce the storage  
 73 that the image takes, and to lessen the time it takes to transmit the image data in the medical field,  
 74 the development in specialized-medical lossy compression technique is in need. This paper focuses  
 75 on lossy compression using the Singular Value Decomposition. Also, the applications of image com-  
 76 pression based on SVD in the medical field are explicated in the contents below. The objective of  
 77 this paper is to propose an optimal rank for each medical image, considering their characteristics  
 78 so that there is no visual difference between the original image and the compressed image and the  
 79 compressed image has a relatively small data size. We also propose a new approach for the lossy  
 80 compression technique for medical imaging compression using Singular Value Decomposition (SVD).  
 81

82 The following consist of Methods, Result, and Conclusion. In the Methods part, Singular Value  
 83 Decomposition is mathematically illustrated with one figure, and the image quality assessment met-  
 84 rics such as L1/L2 error, SSIM, and PSNR are introduced with the formula. In the Result part,  
 85 how the rank of the truncation affects the image quality is analyzed and the optimal rank of each  
 86 image is chosen with appropriate metrics.

## 87 **2 Methods**

### 88 **2.1 Singular Value Decomposition**

89 Singular Value Decomposition, or SVD, is one of the most widely used matrix factorization tech-  
 90 niques. The theoretical illustration is the following:  
 91

92 Let  $X$  be an arbitrary  $M \times N$  matrix. Then, after applying SVD to this matrix  $X$ , we can gener-  
 93 ate three distinct matrices  $U, \Sigma, V^T$ . To illustrate Singular Value Decomposition in mathematical  
 94 expression,

$$X = U \Sigma V^T \quad (1)$$

95 Once generating  $X^T X$ , we can find corresponding eigenvalues  $\lambda_1 \geq \lambda_2 \geq \dots \geq \lambda_n \geq 0$  and normal-  
 96 ized eigenvectors  $v_1, v_2, \dots, v_n$ .

$$V = [v_1 \quad v_2 \quad \dots \quad v_n] \quad (2)$$

As above,  $V^T$ , the right singular value matrix, corresponds to the orthonormal matrix that consists  
 of normalized eigenvectors of  $X^T X$ .

$$\Sigma = \begin{bmatrix} \sigma_1 & 0 & \dots & 0 \\ 0 & \sigma_2 & \dots & 0 \\ 0 & 0 & \dots & \sigma_n \end{bmatrix} \quad (3)$$

97

98  $\Sigma$ , the singular value matrix, is the diagonal matrix where its diagonals are the square root of non-  
99 zero eigenvalues of  $X^T X$  in descending order. In this matrix, the characteristic of the diagonal  
100 entries can be written as follows:  $\sigma_1 = \sqrt{\lambda_1} \geq \sigma_2 = \sqrt{\lambda_2} \geq \dots \geq \sigma_n = \sqrt{\lambda_n}$ .

101

102  $U$ , the left singular value matrix, is also an orthonormal matrix. And, the rank of the matrix  
103  $X$  is also equal to the number of non-zero singular values. Let  $r$  be the rank of the matrix  $X$ .

$$U = [u_1 \ u_2 \ \dots \ u_r] \quad \text{where } u_p = \frac{1}{\sigma_p} X v_p, \ p \in \mathbb{Z}, \text{ and } 1 \leq p \leq r \quad (4)$$

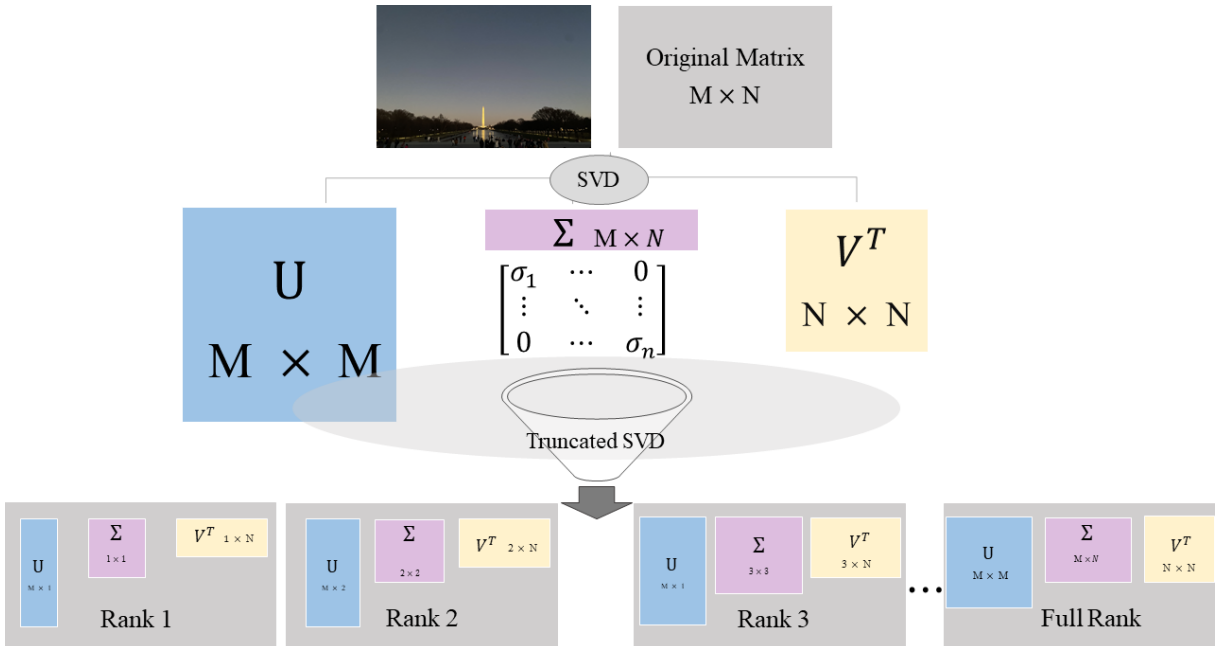


Figure 1: Caption

104 **2.2 Image Compression**

105 **2.2.1 Image Compression Based on SVD**

106 Since every medical image is stored in and transmitted through digital devices, the image matrix  
107 represents the image that's displayed on the device. Every digital image has its own pixel matrix  
108 that has a value assigned from 0 to 255 for each pixel according to the characteristic of the image.  
109 Thus, with the fact that images are stored in the form of matrices in the digital devices, we can  
110 apply Singular Value Decomposition to compress the medical image. Once we extract the target  
111 image in matrix form, the image pixel matrix  $A$  can be factorized into three matrices  $U, \Sigma, V^T$  so  
112 that the number of the singular values, or the rank, could be controlled by the experimenter.

113

114 The truncated SVD works as follows:

115 Let  $k$  be the rank selected to be tested. Then,  $\Sigma$  becomes  $k \times k$  matrix,  $U$  becomes  $m \times k$  matrix,  
116 and  $V$  becomes  $n \times k$  matrix. Then, the size of the truncated image becomes the sum of these three  
117 matrices.

$$\text{size of the rank } k \text{ truncation image} = k(n + 1 + m) \quad (5)$$

118 **2.2.2 Optimal Rank**

119 To decide the optimal rank of the image compression, the metrics to measure the quality of the  
120 image need to be abstracted. L1/ L2 error, relative errors, PSNR and SSIM are used in this paper.

121 • L1/L2 Error and Relative Error

122 L1 error is the sum of the absolute difference of the original image's pixel value and the truncated  
123 image's pixel value. The formula is as follows:

$$\sum_{i=0}^{m-1} \sum_{j=0}^{n-1} |P_{ij} - P'_{ij}| \quad (6)$$

124 where  $P_{ij}$  is the pixel value of the original image and  $P'_{ij}$  is the pixel value of the SVD truncated  
125 image.

126

127 L2 error is the sum of the square of the differece of the original image's pixel and the truncated  
128 image's pixel. The formula is as follows:

$$\sum_{i=0}^{m-1} \sum_{j=0}^{n-1} (P_{ij} - P'_{ij})^2 \quad (7)$$

129 where  $P_{ij}$  is the pixel value of the original image and  $P'_{ij}$  is the pixel value of the SVD truncated  
130 image.

131

132 In our paper, relative error for L1 error is defined to be the sum of the absolute value of the

<sup>133</sup> error difference divided by the standard deviation of the original image. The formula is as follows:

$$\sum_{n=1}^{r_{ori}-1} \frac{|e_{n+1} - e_n|}{\sigma} \quad (8)$$

<sup>134</sup> where  $r_{ori}$  is the rank of the original image,  $e_n$  is the L1 error at rank n, and  $\sigma$  is the standard  
<sup>135</sup> deviation of the original image.

<sup>136</sup>

<sup>137</sup> Similarly, relative error for L2 is defined to be the sum of the absolute value of the error differ-  
<sup>138</sup> ence divided by the standard deviation of the original image. The formula is as follows:

$$\sum_{n=1}^{r_{ori}-1} \frac{|e_{n+1} - e_n|}{\sigma} \quad (9)$$

<sup>139</sup> where  $r_{ori}$  is the rank of the original image,  $e_n$  is the L2 error at rank n, and  $\sigma$  is the standard  
<sup>140</sup> deviation of the original image.

<sup>141</sup> • PSNR: Peak Signal-to-Noise Ratio

<sup>142</sup> PSNR is a metric that uses the concept of the mean square error to compare the quality of the  
<sup>143</sup> image. To get MSE of  $M \times N$  image(matrix), we need to use this formula :

$$\sum_{i=0}^{m-1} \sum_{j=0}^{n-1} \frac{(P_{ij} - P'_{ij})^2}{MN} \quad (10)$$

<sup>144</sup> where  $P_{ij}$  is the pixel value of the original image and  $P'_{ij}$  is the pixel value of the SVD truncated  
<sup>145</sup> image. The Peak signal-to-noise ratio is a commonly used quality assessment technique to measure  
<sup>146</sup> the quality of reconstruction of lossy image compression. The signal is considered as the original  
<sup>147</sup> image data and the noise is the error caused by the compression. The PSNR also reflects human  
<sup>148</sup> perception on the image compression. PSNR value ranges from 30 to 50 dB for 8-bit data and from  
<sup>149</sup> 60 to 80 dB for 16-bit data. [13] The formula for PSNR is as follows:

$$10 \log_{10} \left( \frac{R^2}{MSE} \right) \quad (11)$$

<sup>150</sup> where R corresponds to the maximum pixel value of the image data and MSE is the mean square  
<sup>151</sup> error given by Equation (10).

<sup>152</sup> • SSIM: Structural Similarity Index

<sup>153</sup> SSIM(Structural Similarity Index) Method is also a image assessment metric based on perception. In  
<sup>154</sup> this method, we consider image degradation as the change of perception in structural information.[14]  
<sup>155</sup> Given two images x and y to be original image and truncated image, *luminance* is the mean of each  
<sup>156</sup> image which is given as follows:

$$\mu_x = \frac{1}{N} \sum_{x=1}^N x_n \quad (12)$$

<sup>157</sup> *contrast* uses the standard deviation formula as follows:

$$\sigma_x = \sqrt{\frac{1}{N-1} \sum_{n=1}^N (x_n - \mu_x)^2} \quad (13)$$

<sup>158</sup> and *structure* is given as:

$$\zeta_x = \frac{x - \mu_x}{\sigma_x}. \quad (14)$$

<sup>159</sup> Then, SSIM is calculated with a luminance comparison function, a contrast comparison function,  
<sup>160</sup> and a structure comparison function. The formula is described as:

$$SSIM(x, y) = l(x, y)^\alpha \cdot c(x, y)^\beta \cdot s(x, y)^\gamma \quad (15)$$

<sup>161</sup> where

$$l(x, y) = \frac{2\mu_x\mu_y + C_1}{\mu_x^2 + \mu_y^2 + C_1} \quad (16)$$

<sup>162</sup>

$$c(x, y) = \frac{2\sigma_x\sigma_y + C_2}{\sigma_x^2 + \sigma_y^2 + C_2} \quad (17)$$

<sup>163</sup>

$$s(x, y) = \frac{\sigma_{xy} + C_3}{\sigma_x\sigma_y + C_3} \quad (18)$$

<sup>164</sup> This paper assigns the most common setting as  $\alpha = \beta = 1$  and  $C_3 = C_2/2$  which yields SSIM to be  
<sup>165</sup> as follows [15] :

$$SSIM(x, y) = \frac{(2\mu_x\mu_y + C_1)(2\sigma_{xy} + C_2)}{(\mu_x^2 + \mu_y^2 + C_1)(\sigma_x^2 + \sigma_y^2 + C_2)}. \quad (19)$$

### <sup>166</sup> 2.3 Applications: Medical Image

<sup>167</sup> In this paper, 4 MRI images and 4 X-ray images have been used for the image compression. The  
<sup>168</sup> images are zero-padded for equivalent condition. We use these zero-padded medical images to apply  
<sup>169</sup> the Singular Value Decomposition as described in Figure 1. Afterwards, we execute the low rank  
approximation and reconstruct the truncated image.

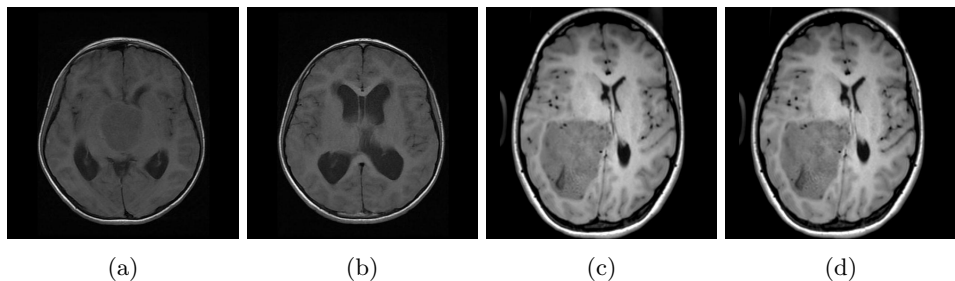
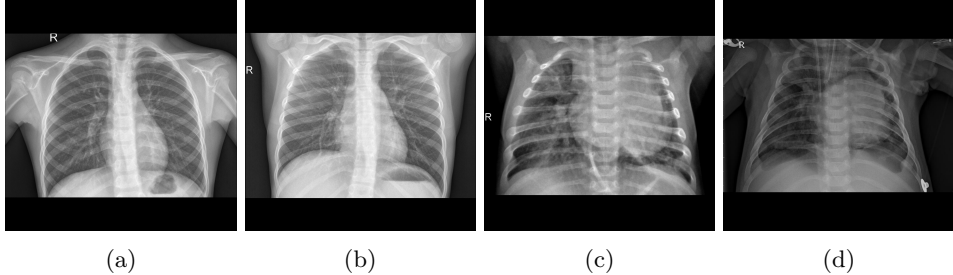


Figure 2: These are 4 MRI images used in this paper.

<sup>170</sup>  
<sup>171</sup> For the qualitative approach, the difference images between the original images and the optimally  
<sup>172</sup> compressed images are extracted. Difference images are constructed as follows: Let  $p_{mn}$ (original)



(a) (b) (c) (d)

Figure 3: These are 4 X-ray images used in this paper.

be the pixel value of the original image in  $m^{th}$  row and  $n^{th}$  column. And, Let  $p_{mn}(\text{optimal})$  be the pixel value of the svd compressed image in the  $m^{th}$  row and  $n^{th}$  column. Then, we take the difference of each image pixel and create a difference matrix.

For the quantitative approach, different kinds of image quality assessment metrics are used. The rank that makes its reconstructed image's SSIM larger than 0.95 and 0.99 are respectively observed. And corresponding L1/L2 error, relative errors, PSNR are extracted and analyzed. This paper will suggest an optimal rank of the SVD image composition that remains high in similarity with the original image and takes less storage than the original image.

### 3 Result

#### 3.1 Optimal Rank for Medical Image Compression on SVD

The optimal rank for medical image compression based on SVD has been chosen based on SSIM in this paper. Two thresholds are set: SSIM > 0.95 and SSIM > 0.99.

##### 3.1.1 MRI Images

	$r_{ori}$	$r_{opt}$	PSNR	$\frac{r_{opt}}{r_{ori}}$
2-(a)	473	55	37.9593872818052	0.1162790698
2-(b)	473	59	38.561411231756	0.1247357294
2-(c)	511	60	39.7522287499315	0.1174168297
2-(d)	512	60	39.6538543950581	0.1171875

Table 1: This is a table containing the results for the 4 compressed MRI images with the optimal rank 5 where  $r_{opt}$  is the optimal rank based on the observation of SSIM > 0.95 and  $r_{ori}$  is the original rank of the image.

For the optimization based on SSIM > 0.95, corresponding PSNR values ranged from 37 dB to 40 dB and it increases as the original rank is higher. The ratio  $\frac{r_{opt}}{r_{ori}}$  show that about 11% of the singular values are used in optimization for 4 MRI images. And, 4 images below are the difference images constructed based on the description in the Method part. There are some differences presented in the contour of the objectives of 4 MRI images but no significant difference is found.

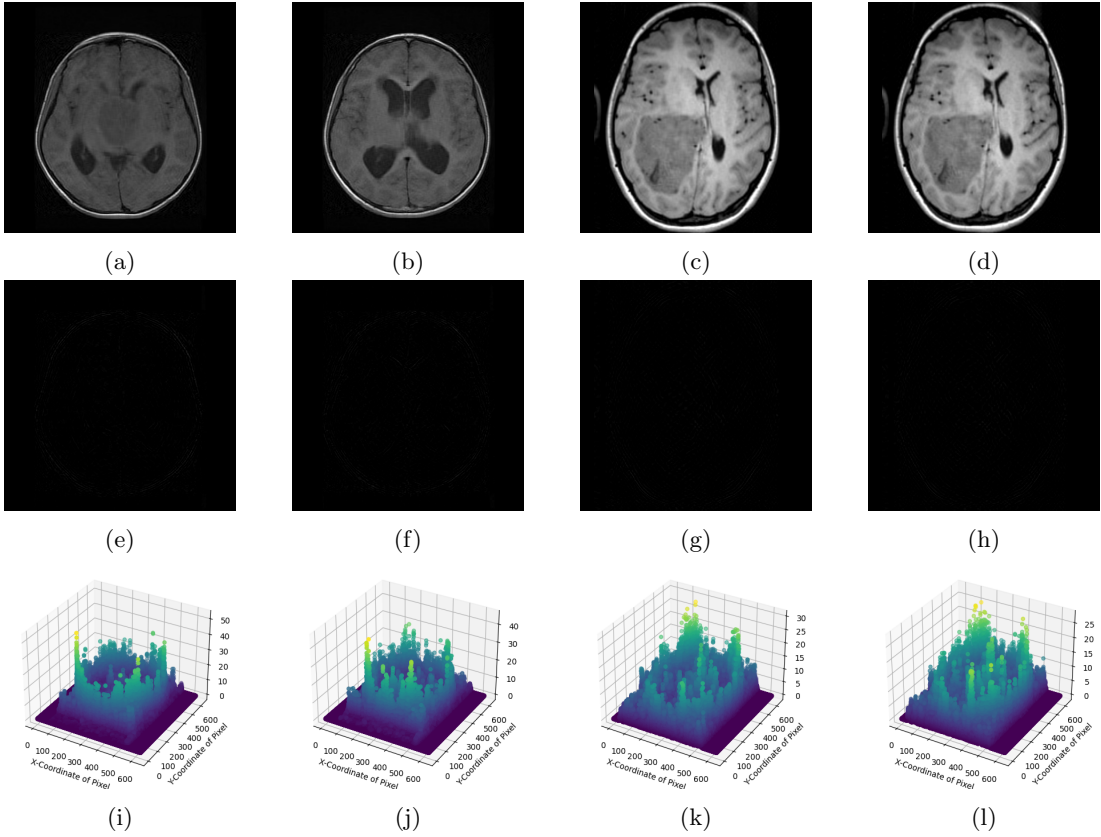


Figure 4: (a)~(d) are compressed images, (e)~(h) are difference images, and (i)~(l) are scatter plots for the difference of pixel values of 4 MRI images when optimized with  $\text{SSIM} > 0.95$ .

	$r_{ori}$	$r_{opt}$	PSNR	$\frac{r_{opt}}{r_{ori}}$
2-(a)	473	100	47.7405542704281	0.2114164905
2-(b)	473	103	47.5215627756651	0.2177589852
2-(c)	511	91	47.0891781543897	0.1780821918
2-(d)	512	90	46.9322872134835	0.17578125

Table 2: This is a table containing the results for the 4 compressed MRI images with the optimal rank 5 where  $r_{opt}$  is the optimal rank based based on the observation of  $\text{SSIM} > 0.99$  and  $r_{ori}$  is the original rank of the image.

191

192 For the optimization based on  $\text{SSIM} > 0.99$ , corresponding PSNR values ranged from 46 dB to 48  
 193 dB and it has a tendency to increase as the original rank is higher. The ratio  $\frac{r_{opt}}{r_{ori}}$  shows that about  
 194 20% of the singular values are used in optimization for 4 MRI images. For the difference images  
 195 below, there is no significant difference between the original image and the compressed image other  
 196 than some trivial differences in texture.

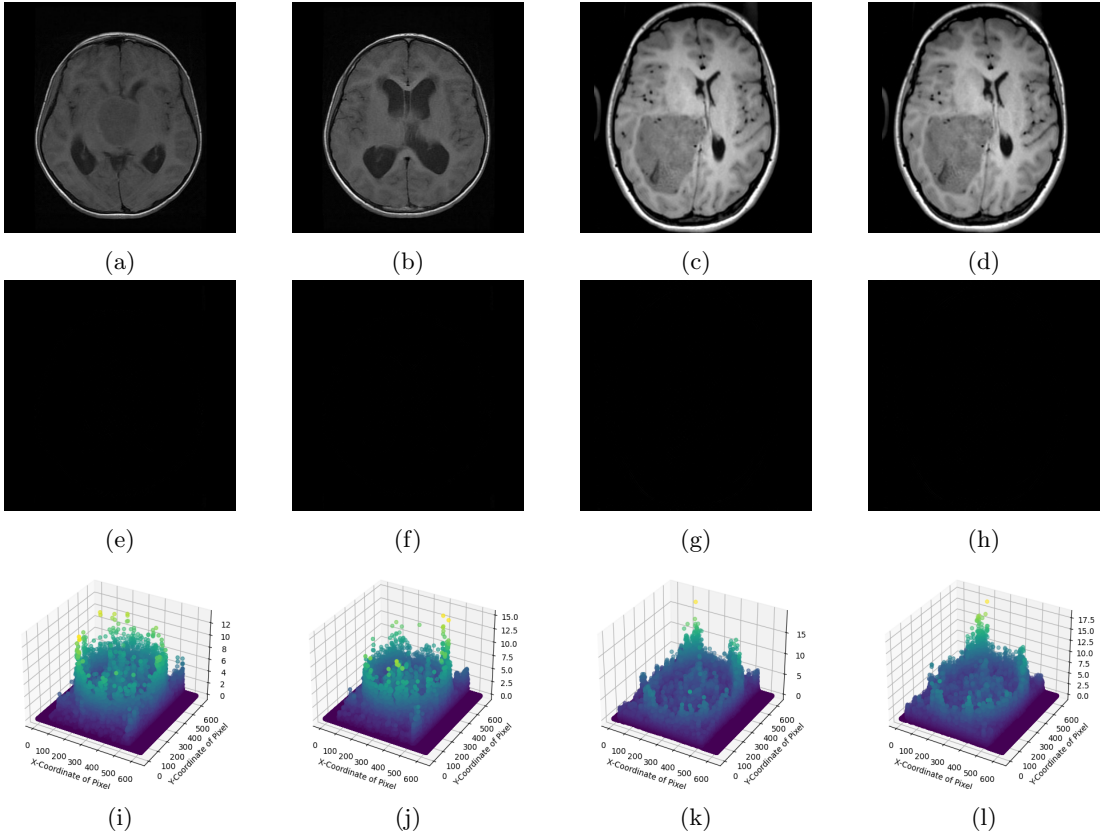


Figure 5: (a)~(d) are compressed images, (e)~(h) are difference images, and (i)~(l) are scatter plots for the difference of pixel values of 4 MRI images when optimized with SSIM > 0.99.

197 For further approach, we explored the region of errors for each image. The method is that  
 198 the 75<sup>th</sup> percentile value of the total error serves as the threshold and the pixel that has a larger  
 199 error than the threshold is marked white in the zero image of the same size as each original image.  
 200 And, the 3D error plot graphs for each image after removing the errors above the threshold are  
 201 provided below. For every MRI image, it can be analyzed that the errors with especially high values  
 202 occur in the cranial bone which does not impact the anatomical information or the region of interest.  
 203 Moreover, the revised 3D error plots numerically imply that the previous error graphs are dominated  
 204 by extreme error values caused by the region that does not impact the region of interest.

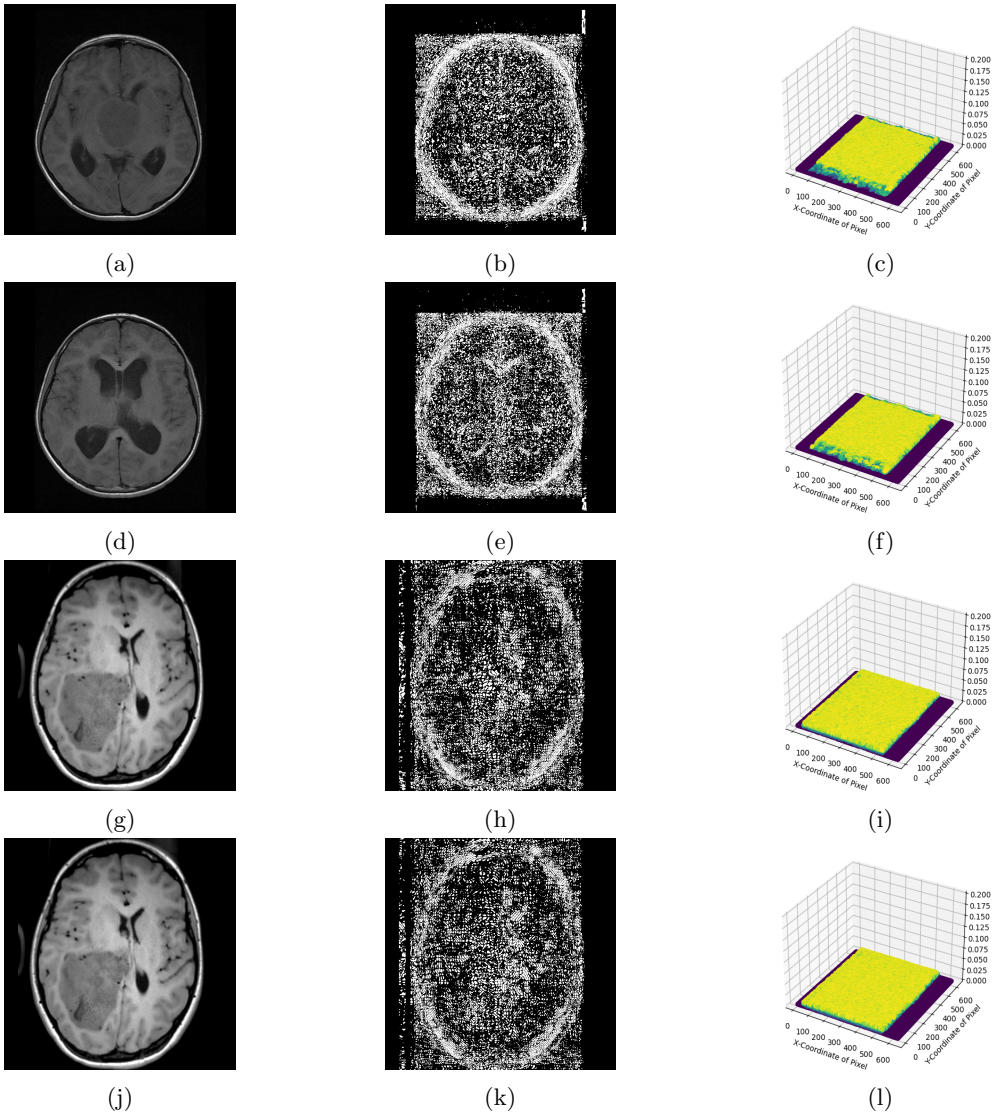


Figure 6: For optimization SSIM  $\geq 0.95$ , (a)~(c) are 2-(a), the error figure that has been constructed with the criteria above, and the revised 3D error plot each. (d)~(f) are 2-(b), the error figure, and the revised 3D error plot each. (g)~(i) are 2-(c), the error figure, and the revised 3D error plot each. (j)~(l) are 2-(d), the error figure, and the revised 3D error plot each.

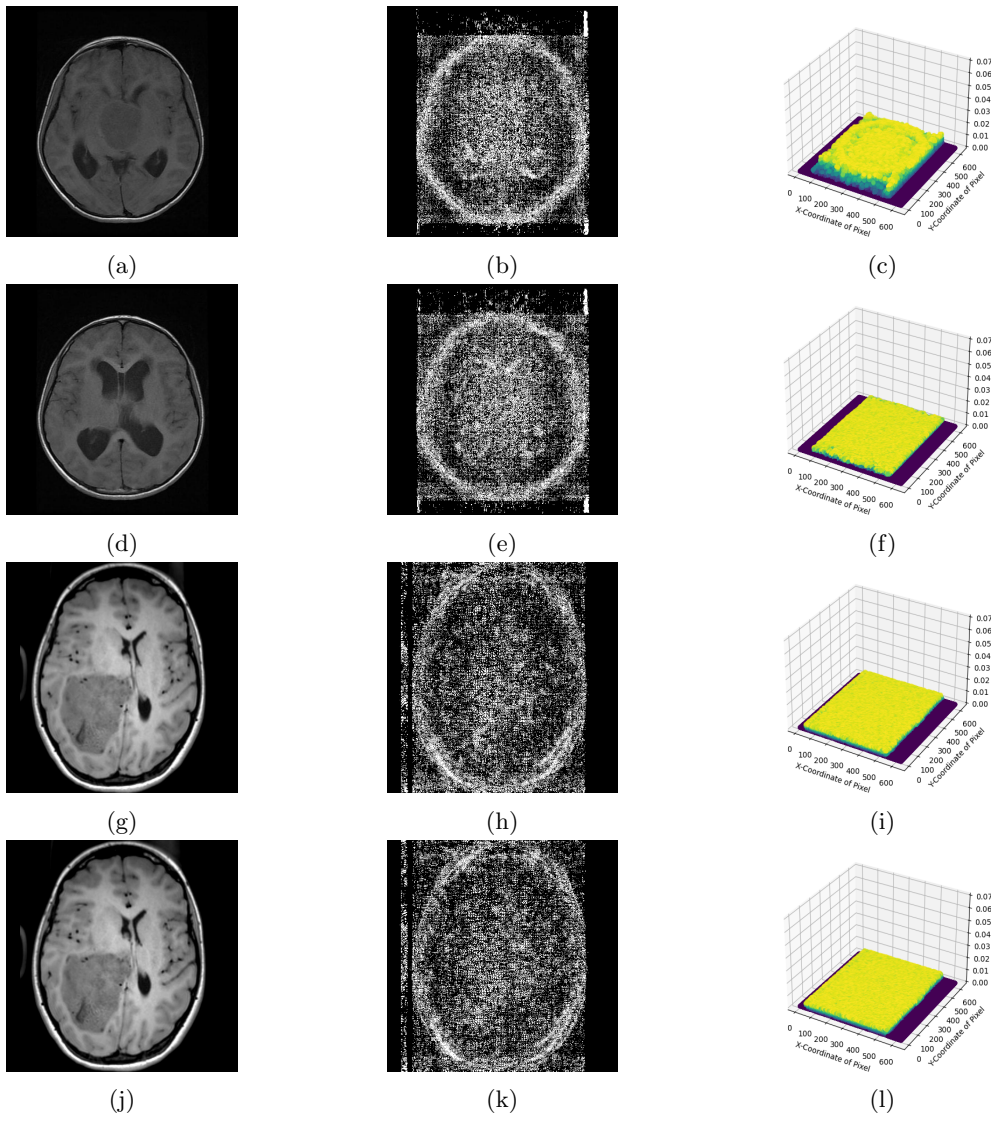


Figure 7: For optimization SSIM  $\geq 0.99$ , (a)~(c) are 2-(a), the error figure that has been constructed with the criteria above, and the revised 3D error plot each. (d)~(f) are 2-(b), the error figure, and the revised 3D error plot each. (g)~(i) are 2-(c), the error figure, and the revised 3D error plot each. (j)~(l) are 2-(d), the error figure, and the revised 3D error plot each.

205    **3.1.2 X-ray Images**

	$r_{ori}$	$r_{opt}$	PSNR	$\frac{r_{opt}}{r_{ori}}$
3-(a)	1317	493	41.1560756946181	0.1579347
3-(b)	1509	571	41.332631388226	0.160371107
3-(c)	762	217	40.641793985265	0.102362205
3-(d)	680	199	40.1265089685621	0.098529412

Table 3: This is a table containing the results for the 4 compressed X-ray images with the optimal rank where  $r_{opt}$  is the optimal rank based on the observation of SSIM  $> 0.95$  and  $r_{ori}$  is the original rank of the image

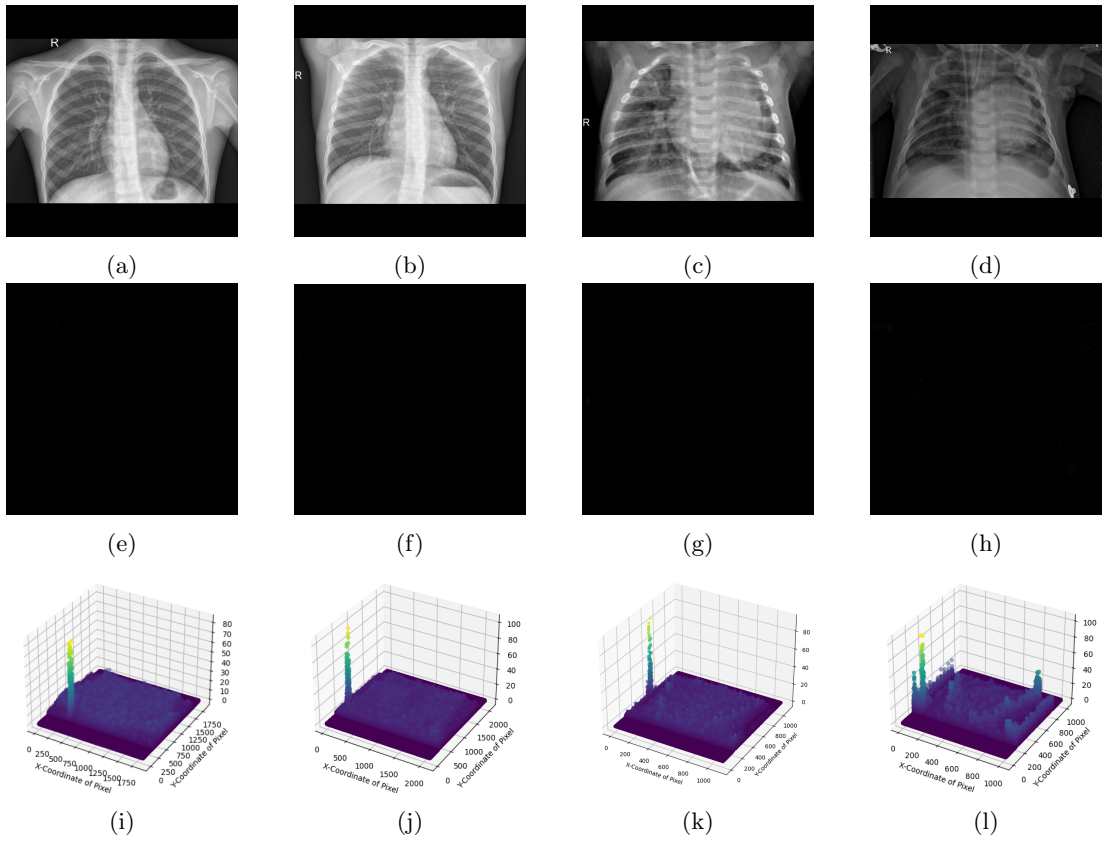


Figure 8: (a)~(d) are compressed images, (e)~(h) are difference images, and (i)~(l) are scatter plots for the difference of pixel values of 4 X-ray images optimized with SSIM  $> 0.95$ .

206    For the optimization based on SSIM  $> 0.95$ , corresponding PSNR values ranged from 40 dB to  
 207    42 dB and it has tendency to increase as the original rank is higher. The ratio  $\frac{r_{opt}}{r_{ori}}$  show that about  
 208    10% to 15% of the singular values are used in optimization for 4 X-ray images. And, 4 images below  
 209    are the difference images constructed based on the description in the Method part. There is no  
 210    significant difference between the original image and the compressed image. There only exists some  
 211    texture difference.

	$r_{ori}$	$r_{opt}$	PSNR	$\frac{r_{opt}}{r_{ori}}$
3-(a)	1317	208	48.2505290660966	0.374335611
3-(b)	1509	242	48.383441712362	0.378396289
3-(c)	762	78	48.1003301244956	0.284776903
3-(d)	680	67	48.4582524720168	0.292647059

Table 4: This is a table containing the results for the 4 compressed X-ray images with the optimal rank where  $r_{opt}$  is the optimal rank based on the observation of SSIM  $> 0.99$  and  $r_{ori}$  is the original rank of the image

212

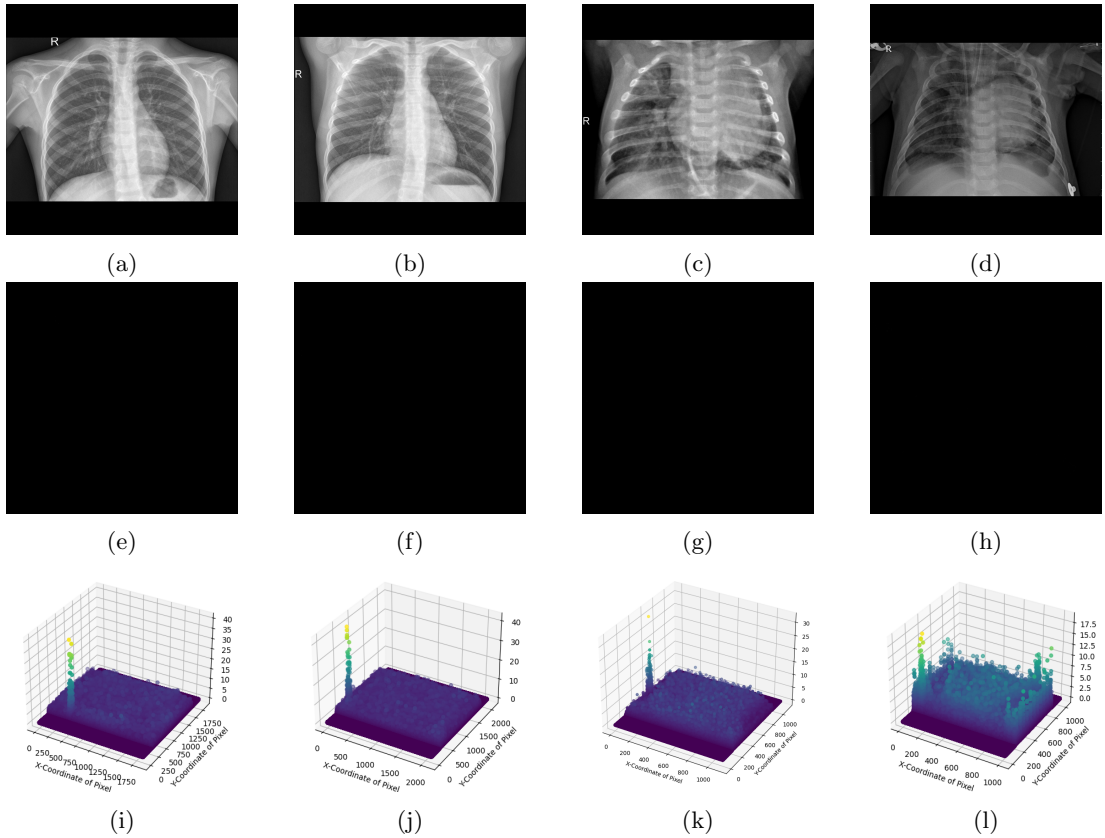


Figure 9: (a)~(d) are compressed images, (e)~(h) are difference images, and (i)~(l) are scatter plots for the difference of pixel values of 4 X-ray images optimized with SSIM  $> 0.99$

213 For the optimization based on SSIM  $> 0.99$ , corresponding PSNR values are around 48 dB and  
 214 it has tendency to increase as the original rank is higher. The ratio  $\frac{r_{opt}}{r_{ori}}$  show that about 30% to  
 215 37% of the singular values are used in optimization for 4 X-ray images. And, for 4 difference images  
 216 below, there is no significant difference between the original image and the compressed image. There  
 217 only exists a trivial texture difference.

218 We have also explored the region of errors for each X-ray image. The same method as MRI images  
 219 has been set to derive the threshold. And, the 3D error plot graphs for each image after removing  
 220 the errors above the threshold are provided below. For every X-ray image, it can be analyzed that  
 221 the errors with especially high values occur at the region where "R" or "L" are located which does  
 222 not impact the anatomical information or the region of interest. Moreover, the revised 3D error  
 223 plots numerically prove that the original error graphs are dominated by extreme error values caused  
 224 by the region that does not impact the region of interest.

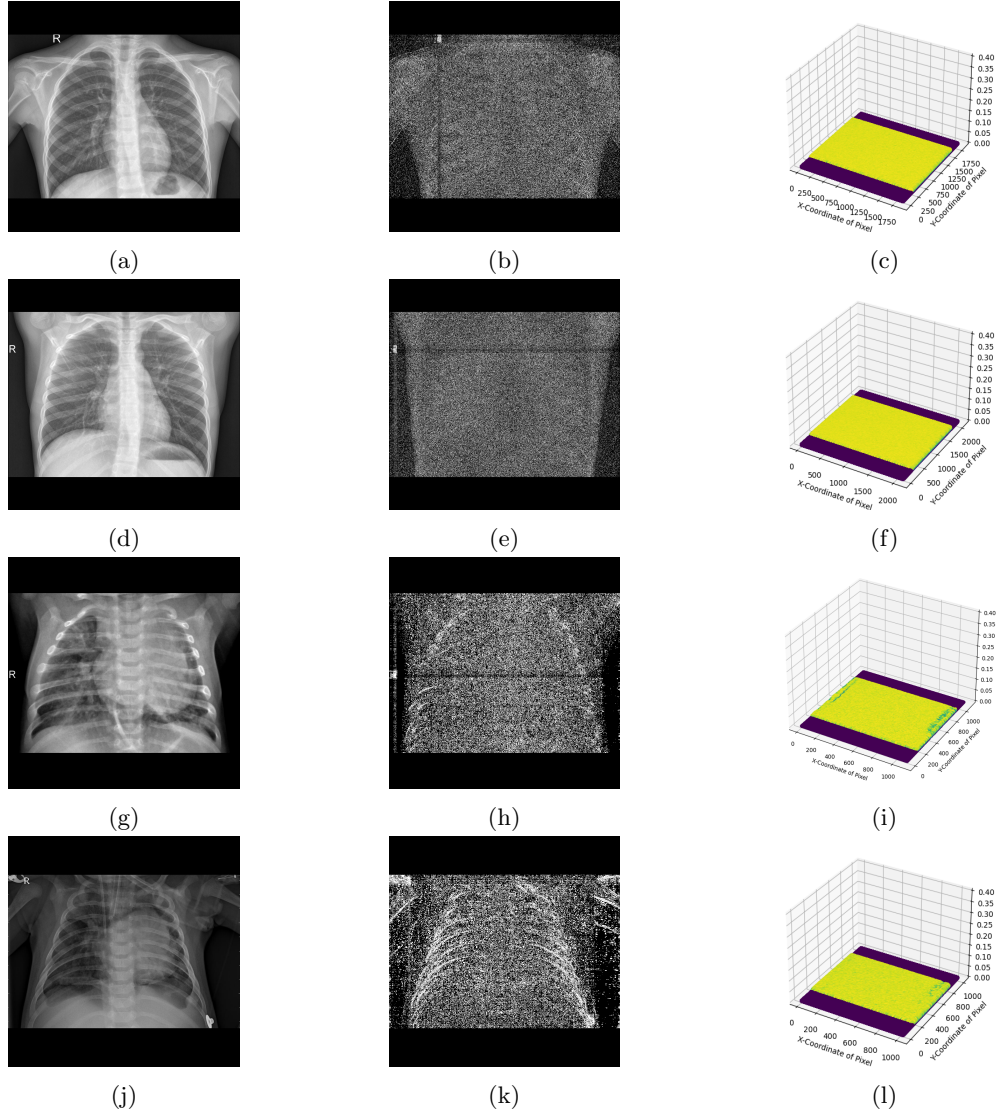


Figure 10: For optimization SSIM  $\geq 0.95$ , (a)~(c) are 3-(a), the error figure that has been constructed with the criteria above, and the revised 3D error plot each. (d)~(f) are 3-(b), the error figure, and the revised 3D error plot each. (g)~(i) are 3-(c), the error figure, and the revised 3D error plot each. (j)~(l) are 3-(d), the error figure, and the revised 3D error plot each.

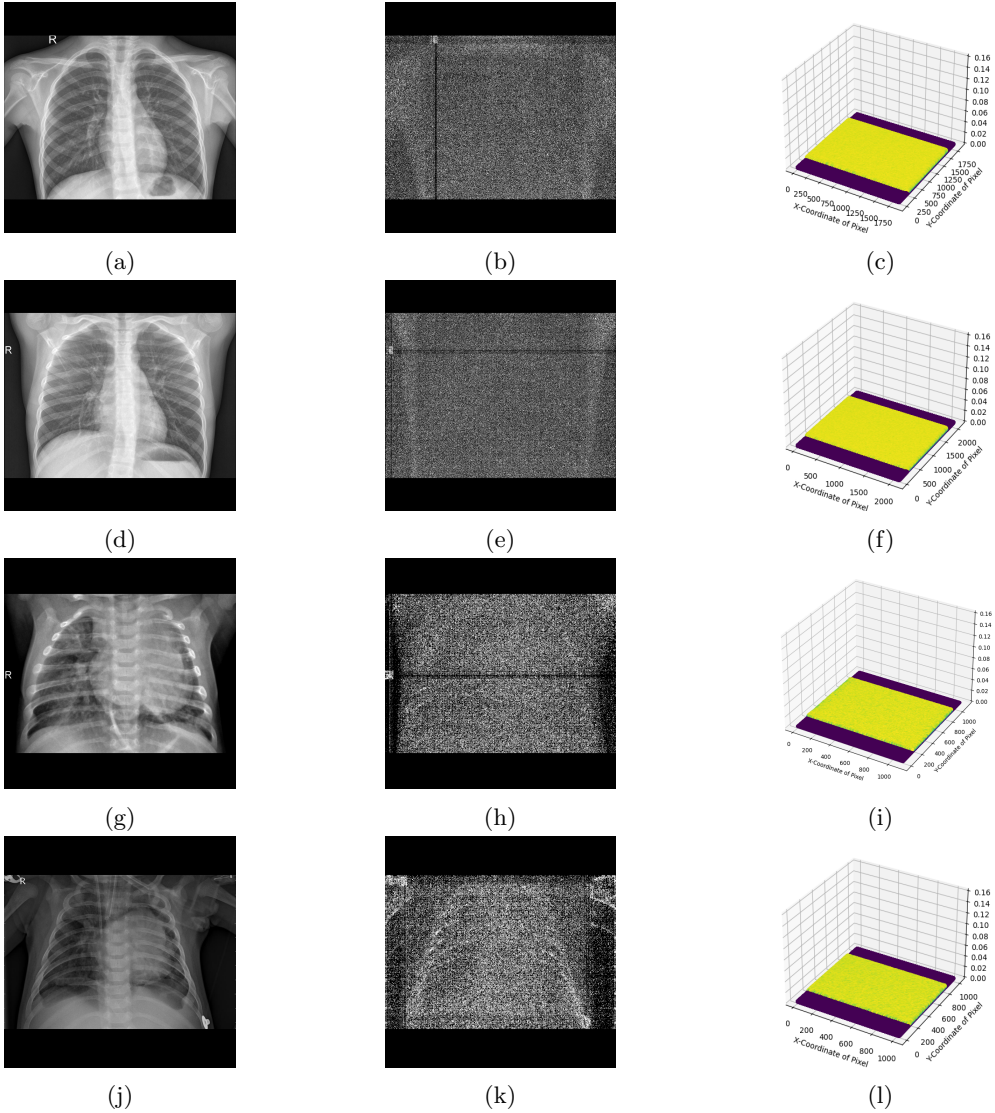


Figure 11: For optimization SSIM  $\geq 0.99$ , (a)~(c) are 3-(a), the error figure that has been constructed with the criteria above, and the revised 3D error plot each. (d)~(f) are 3-(b), the error figure, and the revised 3D error plot each. (g)~(i) are 3-(c), the error figure, and the revised 3D error plot each. (j)~(l) are 3-(d), the error figure, and the revised 3D error plot each.

### 225 3.2 L1/ L2 error and Relative L1/L2 Error

226 4 figures below clearly show that the L1/L2 errors and relative L1/L2 errors of 4 MRI images decay  
 227 faster until some specific ranks and converge to zero slowly after that point. That specific rank  
 228 proves that the errors are saturated at some point of truncation. Thus, it provides feasibility to  
 229 choose an optimal rank of truncation using SVD. Specifically, the red dotted lines represent the  
 230 optimal rank at SSIM  $> 0.95$  and the green dotted lines represent the optimal rank at SSIM  $> 0.99$ .  
 231 The figures verify that the optimal rank is in the range of saturation of the errors.

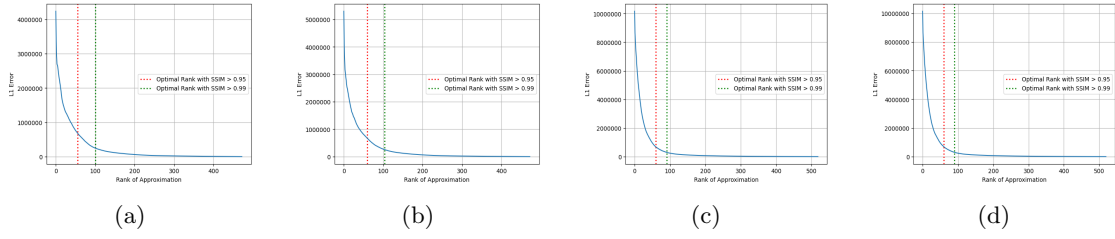


Figure 12: These are graphs for L1 error of 4 MRI images where its x-axis is the rank of truncation and y-axis is the corresponding L1 error

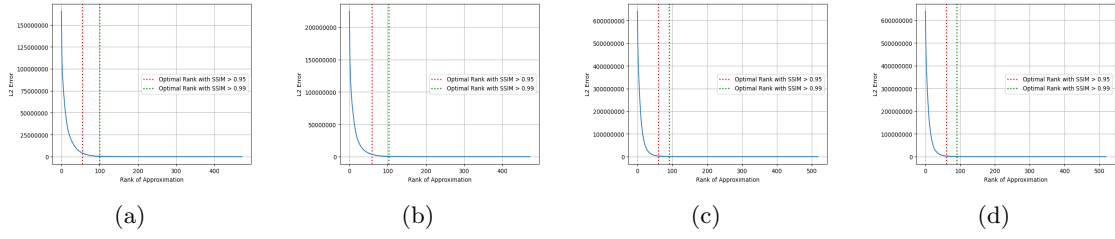


Figure 13: These are graphs for L2 error of 4 MRI images where its x-axis is the rank of truncation and y-axis is the corresponding L2 error

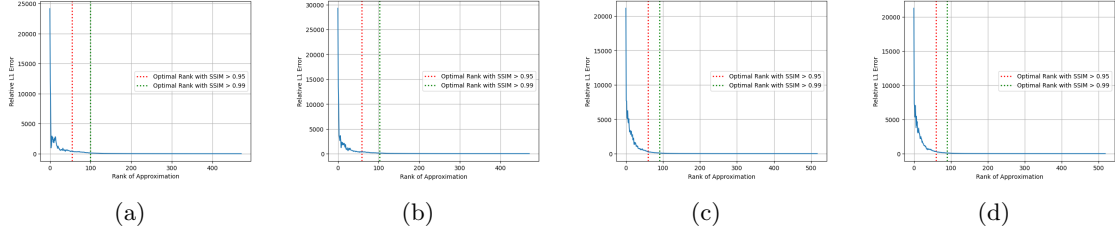


Figure 14: These are graphs for relative L1 error of 4 MRI images where its x-axis is the rank of truncation and y-axis is the corresponding relative L1 error

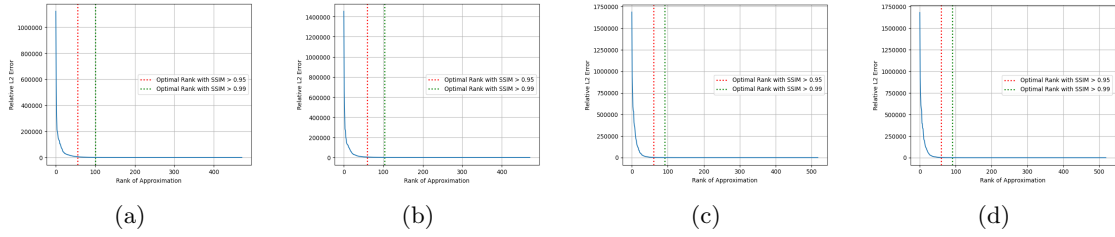


Figure 15: These are graphs for relative L2 error of 4 MRI images where its x-axis is the rank of truncation and y-axis is the corresponding relative L2 error

4 figures below clearly show that the L1/L2 errors and relative L1/L2 errors of 4 X-ray images also decay faster until some specific ranks converge to zero slowly after that point. It is observed that the graphs of X-ray images have a steeper slope of error decay. Therefore, the singular values for X-ray images have more significance in image reconstruction than MRI images.

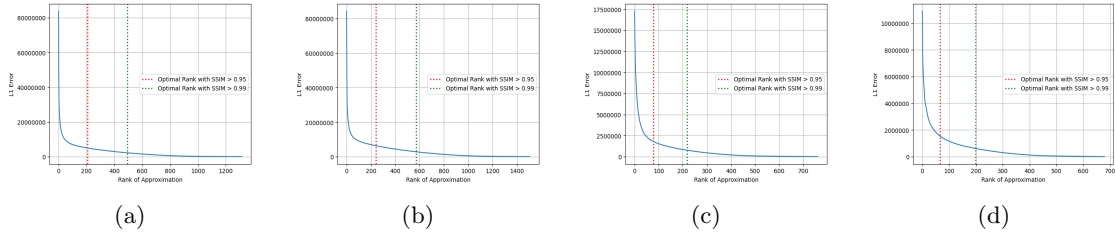


Figure 16: These are graphs for L1 error of 4 X-ray images where its x-axis is the rank of truncation and y-axis is the corresponding L1 error

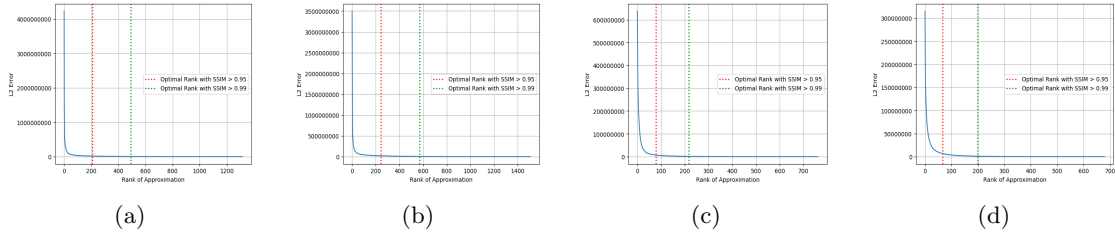


Figure 17: These are graphs for L2 error of 4 X-ray images where its x-axis is the rank of truncation and y-axis is the corresponding L2 error

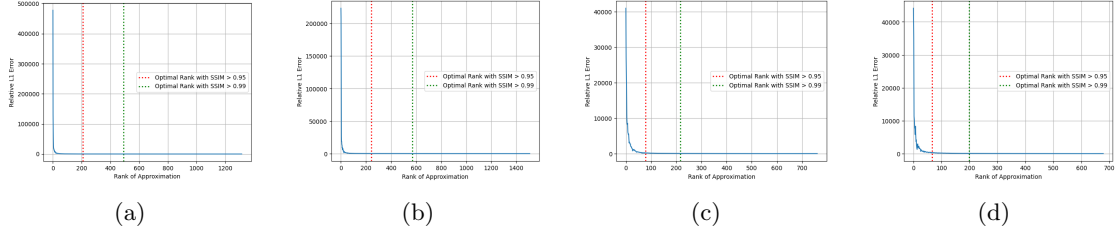


Figure 18: These are graphs for relative L1 error of 4 X-ray images where its x-axis is the rank of truncation and y-axis is the corresponding relative L1 error

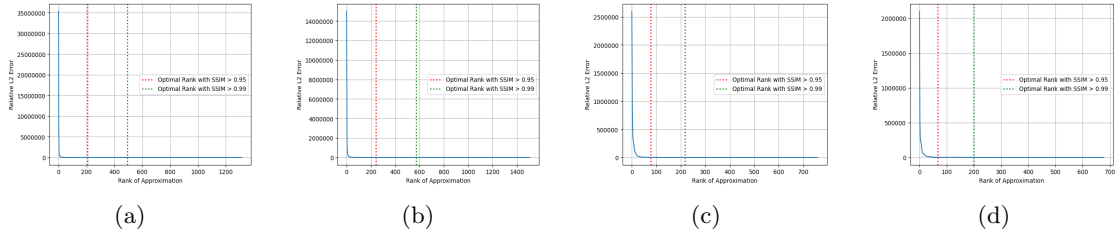


Figure 19: These are graphs for relative L2 error of 4 X-ray images where its x-axis is the rank of truncation and y-axis is the corresponding relative L2 error

### 3.3 SSIM: Structural Similarity Index

The figures below represent the SSIM value of 4 MRI images. SSIM ranges from 0 to 1 and the value that is close to 1 means the compressed image is almost identical with the original image. From these graphs, it is shown that SSIM increases fast until some point and the value converges

240 to 1 slowly. Zinner's research has proven that SSIM scores above 0.99 look perfectly similar to the  
 241 original image, while the compressed images with SSIM in the range from 0.95 to 0.99 range would indicate the presence of perceptible but not interrupting impairments. [16]

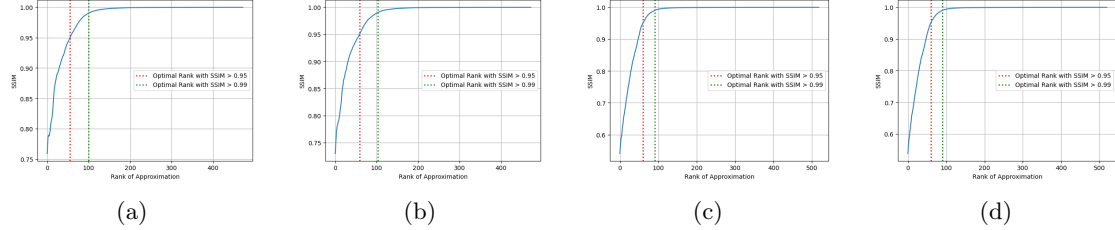


Figure 20: These are graphs for SSIM 4 MRI images where its x-axis is the rank of truncation and y-axis is the corresponding SSIM value

242

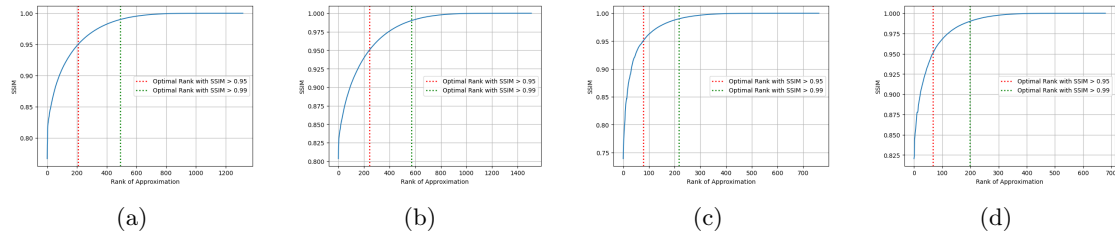


Figure 21: These are graphs for SSIM 4 X-ray images where its x-axis is the rank of truncation and y-axis is the corresponding SSIM value

243

### 3.4 PSNR: Peak Signal-to-Noise Ratio

244 The figure above shows the PSNR value of 4 MRI images. In lossy image compression methods  
 245 such as SVD compression, the compressed image has the PSNR between 30 and 50 dB, where higher  
 246 is better. And, PSNR Values over 40 dB are normally considered to be high in similarity with the  
 247 original image. [17]

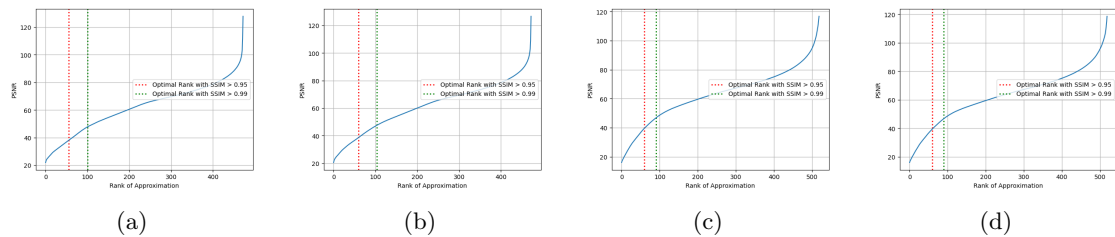


Figure 22: These are graphs for PSNR of 4 MRI images where its x-axis is the rank of truncation and y-axis is the corresponding PSNR value

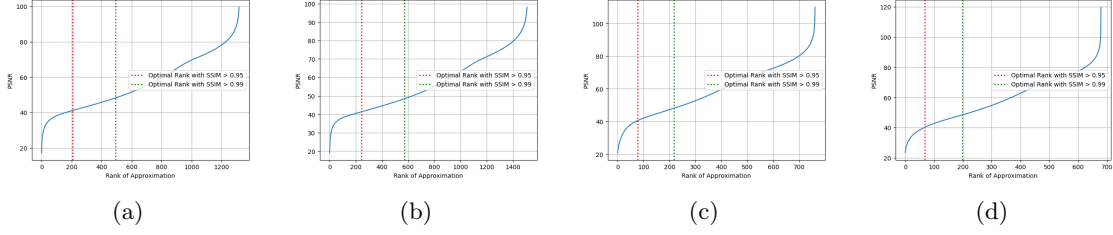


Figure 23: These are graphs for PSNR of 4 X-ray images where its x-axis is the rank of truncation and y-axis is the corresponding PSNR value

### 248 3.5 Comparison: MRI vs X-ray

249 From the results above, it is shown that the overall ratio  $\frac{r_{opt}}{r_{ori}}$  is higher in X-ray. It is interpreted  
 250 that MRI stores more significant information on the first few singular values  $\sigma$  than X-ray. The  
 251 PSNR values ranged higher about 5 dB than MRI in SSIM  $> 0.95$  compression and about 1 dB  
 252 than MRI in SSIM  $> 0.99$  compression. As a result, there are more perceptible differences in MRI  
 253 images than X-ray images.

## 254 4 Conclusion

255 For MRI images, the optimal rank of truncation in SVD image compression would be 10% to  
 256 20% of the original rank. And for X-ray images, the optimal rank of truncation in SVD image  
 257 compression would be 10% to 40% of the original rank. From the results above, we could observe  
 258 that image compression using Singular value Decomposition worked more effectively in X-ray images  
 259 for SSIM  $> 0.95$  truncation. And it is analyzed that the image compression based on SVD worked  
 260 more effectively in MRI images for SSIM  $> 0.99$  truncation. This paper also proposes the significance  
 261 of the number of the singular values in SVD providing valid metrics. With the main threshold SSIM,  
 262 both the qualitative metrics and quantitative metrics have proven the usefulness of SVD in the image  
 263 compression.

## 264 References

- 265 1. Kumar R, Patbhaje U, and Kumar A. An efficient technique for image compression and quality  
 266 retrieval using matrix completion. Journal of King Saud University - Computer and Information  
 267 Sciences 2022;34:1231–9.
- 268 2. Goyal V. Multiple description coding: compression meets the network. IEEE Signal Processing  
 269 Magazine 2001;18:74–93.
- 270 3. Agrawal Jayprakash RV. Compression of MR Images Using DWT by Comparing RGB and  
 271 YCbCr Color Spaces. Journal of Signal and Information Processing 2013;4.
- 272 4. Abduljaleel IQ and Khaleel AH. Significant medical image compression techniques: A Review.  
 273 TELKOMNIKA (Telecommunication Computing Electronics and Control) 2021;19:1612.

- 274 5. Singh M, Kumar S, Chouhan S, and Shrivastava M. Various Image Compression Techniques:  
275 Lossy and Lossless. International Journal of Computer Applications 2016;142:23–6.
- 276 6. Lone MR. A high speed and memory efficient algorithm for perceptually-lossless volumetric  
277 medical image compression. Journal of King Saud University - Computer and Information  
278 Sciences 2022;34:2964–74.
- 279 7. Yee D, Soltaninejad S, Hazarika D, Mbuyi G, Barnwal R, and Basu A. Medical image com-  
280 pression based on region of interest using better portable graphics (BPG). In: *2017 IEEE*  
281 *International Conference on Systems, Man, and Cybernetics (SMC)*. 2017:216–21. DOI: 10.  
282 1109/SMC.2017.8122605.
- 283 8. Monika R and Dhanalakshmi S. An efficient medical image compression technique for telemedicine  
284 systems. Biomedical Signal Processing and Control 2023;80:104404.
- 285 9. Yang F, Pan X, Zhu K, et al. Accelerated 3D high-resolution T2-weighted breast MRI with deep  
286 learning constrained compressed sensing, comparison with conventional T2-weighted sequence  
287 on 3.0 T. European Journal of Radiology 2022;156:110562.
- 288 10. Chen Z, Sun B, Xue Y, et al. Comparing compressed sensing breath-hold 3d Mr Cholangiopan-  
289 creatography with two parallel imaging MRCP strategies in main pancreatic duct and common  
290 bile duct. European Journal of Radiology 2021;142:109833.
- 291 11. Amri H, Khalfallah A, Gargouri M, Nebhani N, Lapayre JC, and Bouhlel MS. Medical image  
292 compression approach based on image resizing, digital watermarking and lossless compression.  
293 Journal of Signal Processing Systems 2016;87:203–14.
- 294 12. BAIRAGI VK and SAPKAL AM. Roi-based DICOM image compression for telemedicine.  
295 Sadhana 2013;38:123–31.
- 296 13. Deshpande R, Ragha L, and Sharma S. Video Quality Assessment through PSNR Estima-  
297 tion for Different Compression Standards. Indonesian Journal of Electrical Engineering and  
298 Computer Science 2018;11:918–24.
- 299 14. Sara U, Akter M, and Uddin MS. Image quality assessment through FSIM, SSIM, MSE and  
300 PSNR—a comparative study. Journal of Computer and Communications 2019;07:8–18.
- 301 15. Brooks AC, Zhao X, and Pappas TN. Structural Similarity Quality Metrics in a Coding Con-  
302 text: Exploring the Space of Realistic Distortions. IEEE Transactions on Image Processing  
303 2008;17:1261–73.
- 304 16. Zinner T, Hohlfeld O, Abboud O, and Hossfeld T. Impact of frame rate and resolution on  
305 objective QoE metrics. In: *2010 Second International Workshop on Quality of Multimedia*  
306 *Experience (QoMEX)*. 2010:29–34. DOI: 10.1109/QoMEX.2010.5518277.
- 307 17. Bull DR and Zhang F. Chapter 4 - Digital picture formats and representations. 2021. Ed. by  
308 Bull DR and Zhang F:107–42.